Polymorphism-Dependent and Switchable Emission of Butterfly-Like Bis(diarylmethylene)dihydroanthracenes

Zikai He,[§,∇,†] Liuqing Zhang,[‡,†] Ju Mei,[§,∇] Tian Zhang,[#] Jacky W. Y. Lam,[§,∇] Zhigang Shuai,[#] Yong Qiang Dong,*[‡] and Ben Zhong Tang*[§,∇]

[‡]Beijing Key Laboratory of Energy Conversion and Storage Materials, Department of Chemistry, Beijing Normal University, No. 19, XinJieKouWai Street, Beijing 100875, China

[§]HKUST-Shenzhen Research Institute, No. 9 Yuexing First RD, South Area Hi-tech Park, Nanshan, Shenzhen 518057, China

[#]Key Laboratory of Organic OptoElectronics and Molecular Engineering, Department of Chemistry, Tsinghua University, Beijing 100084, China

[∇]Department of Chemistry, Division of Life Science, State Key Laboratory of Molecular Neuroscience, Institute for Advanced Study, Institute of Molecular Functional Materials, Division of Biomedical Engineering, The Hong Kong University of Science and Technology, Clear Water Bay, Kowloon, Hong Kong, China

S *Supporting Information*

ABSTRACT: Organic fluorophores with reversible emission switching behavior are promising materials for applications in sensors, optical recording, security inks, and optoelectronics. A variety of aggregation-induced emission (AIE) luminogens with mechanochromic luminescence has been prepared, and the transformation of efficient bluer-emitting crystals to amorphous powders with redder and weaker emission is proposed to be the cause for such behavior. However, detailed mechanistic understanding from experimental to theoretical is lacking. In this work, we present the design and synthesis of a group of bis(diarylmethylene)dihydroanthracenes with butter-fly-like shapes. These molecules exhibit aggregation-induced

emission characteristics due to the restriction of intramolecular motion in the aggregated state. They show mechanochromism, because of the transformation between crystal and amorphous states with different colors and efficiencies aided by grinding/heating or solvent fuming processes. By investigation of their single-crystal structures and theoretical calculations, the loose molecular packing with noncovalent intermolecular interactions, the extent of conformational twisting, and the packing density of the luminogens, as well as freedom of intermolecular motion in the excited state, are stemmed for their reversible polymorphism-dependent emission behaviors.
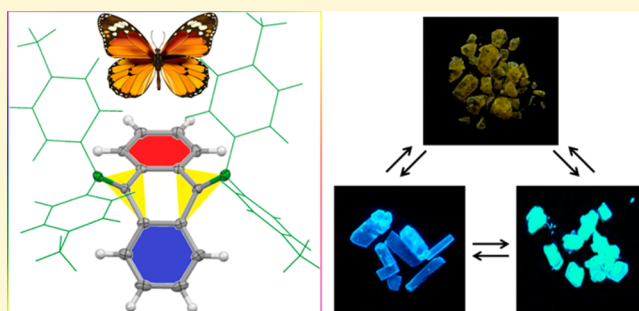
INTRODUCTION

Pure organic mechanochromic materials are a class of smart materials with variable emission[1] in response to mechanical stimuli and have attracted considerable interest not only for fundamental curiosity but also for their practical applications.[2−7] Deciphering the mechanisms of this observed variability is essential for their design and application. Among diverse design strategies, the one with the use and integration of intermolecular noncovalent interactions into luminogenic structure is popular, thanks to its straightforward manipulation, good reversibility, and high efficiency.[8] Changes in molecular conformations and packing modes (polymorphism) will disrupt the intermolecular noncovalent interactions and have been shown to be key factors in influencing the luminescence of most reported dyes.[9−12] However, an in-depth and comprehensive understanding of these claims is difficult, because suitable systems with detailed structural information from experimental to theoretical are lacking.[13−20]

The phenomenon of aggregation-induced emission (AIE) was observed in some luminogens with propeller or shell-like shapes. These molecules were nonemissive when molecularly dissolved in solutions but emitted intensively when their molecules clustered into aggregates.[21−27] What is the cause for such phenomenon? It is well-known that rotation and vibration are two main modes of intramolecular motion accompanied by energy consumption. Recently, we proposed that the AIE effect may mainly originate from the restriction of intramolecular motion (RIM),[28] such as rotation in propeller-like tetraphenyl-ethylene (TPE) and vibration in butterfly-like THBDBA (see Scheme 1).[29,30] In solution, the active intramolecular rotation and vibration have consumed the energy of the excited states through nonradiative relaxation channel, thus rendering the

Scheme 1. Illustration of the AIE Mechanism[a] and Crystal Structure of Bis(diarylmethylene)dihydroathracenes
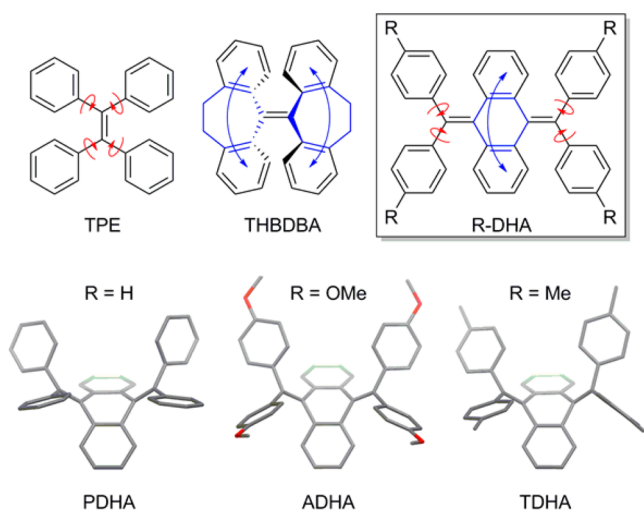
[a]Red arrow indicates rotation; blue arrow indicates vibration.

AIE luminogens nonemissive. Upon aggregation, such motion is restricted, which blocks the nonradiative decay pathway and thus enables the dye molecules to emit intensely. The RIM mechanism is of great importance for extending the AIE scope and enriching the variety of AIE-based functional materials. Most of the AIE luminogens reported so far have been found to exhibit mechanochromic luminescence.[31−35] The discovery of the AIE phenomenon has been considered a key for opening a treasure chest of mechanochromic materials.[1] Unfortunately, a clear explanation on the working mechanism is rarely provided.

In this work, three derivatives of bis(diphenylmethylene)-dihydroanthracene (R-DHA), namely 9,10-bis-(diphenylmethylene)-9,10-dihydroanthracene (PDHA), 9,10-bis(di-4′-methoxylphenylmethylene)-9,10-dihydroanthracene (ADHA), and 9,10-bis(di-4′-methylphenylmethylene)-9,10-di-hydroanthracene (TDHA), with different substituents on the periphery phenyl rings are designed and synthesized. As shown from their crystal structures, these molecules adopt a geometry resembling that of a butterfly, in which the periphery rings serve as rotors, while the central dihydroanthracene blade functions as a vibrator. They are found to exhibit typical AIE effect. For instance, PDHA is induced to emit efficiently when aggregated in the solid state.[36,37] Their mechanochromic, vapochromic, and thermochromic luminescences were studied. By analyzing their crystal structures and results from theoretical calculation, the underlying reasons for fluorescence color and emission changes in the presence of external stimuli are obtained.

■ RESULTS AND DISCUSSION

Synthesis and Photophysical Properties. PDHA, ADHA, and TDHA were facilely synthesized according to the synthetic route shown in Scheme S1 in the Supporting Information, using literature methods with modifications.[38] Starting from 9,10-anthraquinone, grams of products were obtained in high yields under the condition for Corey−Fuchs and Suzuki−Miyaura reactions. All the R-DHAs have good solubility in common organic solvents.

The photophysical properties of PDHA, ADHA, and TDHA are investigated in the solution and aggregated states. All the R-DHAs are virtually nonluminescent when molecularly dissolved

in good organic solvents such as CH_2Cl_2, $CHCl_3$, THF, CH_3CN, toluene, etc., as suggested by the photographs of the solutions taken under UV illumination and the photo-luminescence (PL) spectra shown in Figure 1A, as well as
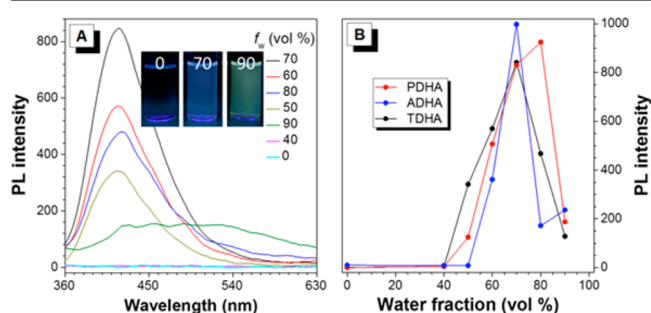
Figure 1. (A) Photoluminescence (PL) spectra of TDHA in CH_3CN/water mixtures with different water fraction (f_w). (B) Plot of PL intensity versus the composition of the CH_3CN/water mixtures of R-DHAs. Concentration = 10 μM.

Figures S1−S3 in the Supporting Information. However, when a large amount of water is added into their solutions, the emission of the R-DHAs is largely enhanced (950-fold for PDHA, 120-fold for ADHA, and 5700-fold for TDHA, respectively). Since water is a nonsolvent for the R-DHAs, their molecules must have been aggregated in water/acetonitrile mixtures with high water contents. Clearly, aggregate formation has induced them to emit efficiently (or, in other words, they are AIE-active) because of the restriction of the phenyl ring rotation and low-frequency vibration of the dihydroanthracene blade in the aggregates.[39−41] Careful inspection of the photoluminescence (PL) spectra of the R-DHAs in CH_3CN/water mixtures reveals that their emission is switched on at a water fraction of ∼50%. Afterward, the PL intensity increases gradually and reaches a maximum value. Further increment of the water fraction leads to a weaker emission. Since all the solutions remain homogeneous without precipitates, the PL decrease at high water content may be due to the morphology change in the aggregates from crystalline to amorphous.[17] It is noteworthy that the emission color changes from blue to green upon gradual water addition, suggesting that the R-DHAs may exhibit polymorphism-dependent lumines-cence properties.

To verify the above speculation, their PL at different states was investigated. The results are summarized in Table 1. The

Table 1. Photophysical Properties of PDHA, ADHA, and TDHA in the Aggregated States

sample	λ_{em}[a] (nm)	Φ_F[b] (%)	Fluorescence Decay			
			A_1/A_2[c] (%)	τ_1 (ns)	τ_2 (ns)	$\langle \tau \rangle$[d] (ns)
PDHA-c	446	15.1	44/56	0.32	1.26	0.85
ADHA-c	420	2.5	63/37	0.09	0.88	0.38
ADHA-am	533	2.2	64/36	0.31	2.38	1.06
TDHA-b	425	27.7	50/50	0.31	1.41	0.86
TDHA-g	464	76.8	0/100		1.86	1.86
TDHA-am	520	3.3	72/28	0.15	1.16	0.43

[a]Emission maximum. [b]Fluorescence quantum yield determined by using a calibrated integrating sphere at an excitation wavelength of 325 nm. [c]Fraction of the shorter (A_1) and longer-lived (A_2) species. [d]Mean lifetime $\langle \tau \rangle$ calculated by using the equation $\langle \tau \rangle = A_1\tau_1 + A_2\tau_2$.

crystals of R-DHAs were obtained by slow diffusion of *n*-hexane into their CHCl$_3$ solutions.[42] Except PDHA, which may possess a good self-recovering or fast crystallization ability, amorphous powders of ADHA and TDHA were obtained by quenching their melts with liquid nitrogen. Crystals of PDHA (abbreviated as PDHA-c) emits blue light at 446 nm with a quantum yield of 15.1%. However, its cousin, ADHA, exhibits a low quantum yield of ∼2%−3% in both crystalline (ADHA-c) and amorphous (ADHA-am) states. Interestingly, two types of TDHA crystals (TDHA-b and TDHA-g) were obtained from its *n*-hexane/CHCl$_3$ mixture. While TDHA-b emits at 425 nm with a quantum yield of 27.7%, TDHA-g exhibits a more efficient redder emission (464 nm and 76.8%). Compared to their crystalline counterparts, the amorphous powders of TDHA (TDHA-am) are weaker emitters, the luminescence of which is observed at a longer wavelength of 520 nm with a lower quantum yield of 3.3%. What are the reasons behind this? It is believed that luminogenic molecules are poorly packed in the amorphous state. This may generate many free spaces for the phenyl rings and dihydroanthracene blade to rotate and vibrate, thus leading to partial emission quenching. On the other hand, because of the free of constraint in the crystal lattice, the molecules in the amorphous powders may assume a more planar conformation and, hence, show a redder emission.[17] It is noteworthy that the quantum yields of ADHA-am and TDHA-am are much lower that those of amorphous powders of TPE derivatives (∼40%),[43] possibly due to their comparative poorer molecular packing, which is caused by their butterfly-like shapes. Lifetime measurement reveals that fluorescence characteristics of the dye molecules and the mean lifetime values are generally in correlation with the observed quantum yields.

Crystallographic Analysis and Polymorphism. We then analyzed the crystal structures of R-DHAs with a view to study their molecular conformation and packing mode[44,45] and, hence, understand their emission behaviors at different aggregated states. Figure 2 show the crystal structure of

Comp.	Ψ_{AB}	Ψ_{CD}
PDHA	132.4°	79.0°
ADHA	131.0°	70.6°
TDHA-b	134.7°	77.7°
TDHA-g	133.5°	73.3°
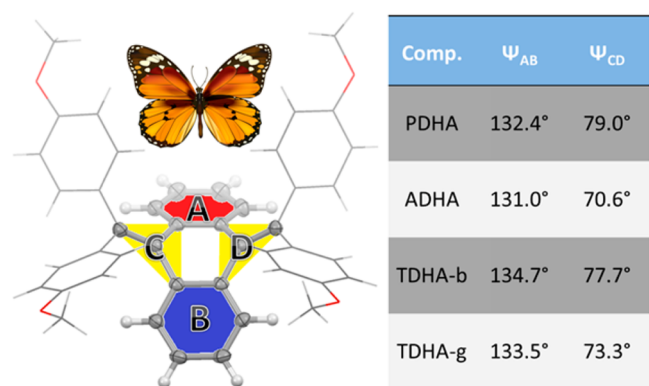
Figure 2. Molecular geometry illustration of the crystal structure of TDHA and summary of the dihedral angles in PDHA, ADHA, and TDHA crystal structures.

ADHA, as an example, where the central dihydroanthracene moiety is bent because of the steric effect of the diaryl-methylene groups. The large dihedral angles between the dihydroanthracene backbone (Ψ_{AB}) and the diarylmethylene groups (Ψ_{CD}) suggest that ADHA adopts a highly contorted structure, which resembles that of a butterfly. The conjugation between the two components becomes very weak. As a result,

blue emission is anticipated. The PDHA and TDHA crystals assume similar distorted structures. Since the dihedral angles in TDHA-b are larger than those in TDHA-g, this should lead to poorer electronic communication and, hence, bluer emission with a lower efficiency.

Closer examination shows that the average volume occupied by a single dye molecule in the crystal lattice is much larger that its molecular size (704.1 Å^3 for PDHA, 1038.6 Å^3 for ADHA, 805.6 Å^3 for TDHA-b, and 778.3 Å^3 for TDHA-g, respectively). This suggests a loosely molecular packing, which should enable the molecules to have some sort of motion. However, multiple CH···HC, CH···C, and C···C interactions are found throughout the crystal structures of R-DHAs (see Figure 3, as well as
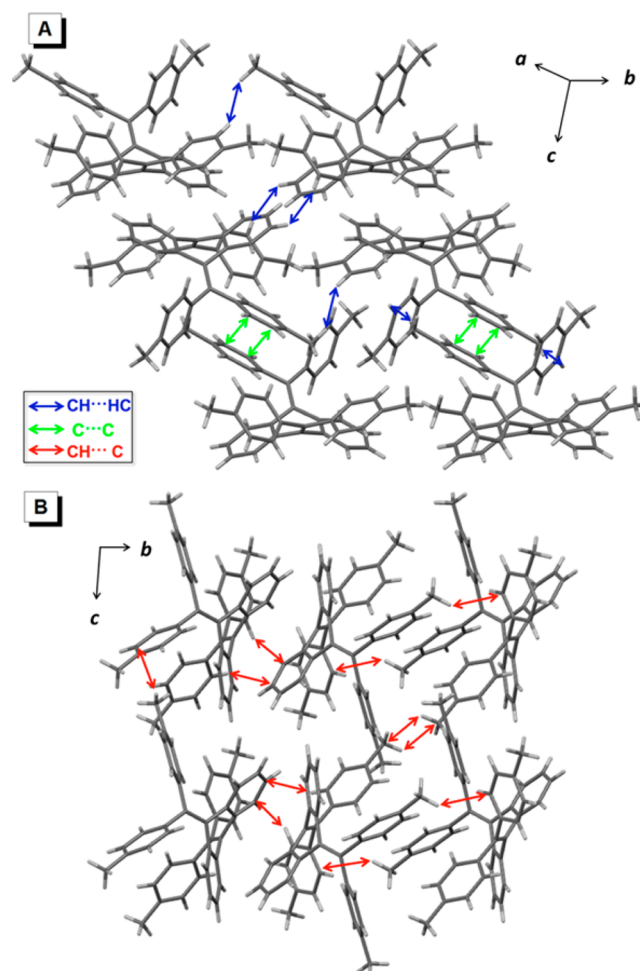
Figure 3. (A) Molecular packing in TDHA-g. (B) Molecular packing in TDHA-b, as viewed along the *a*-axis of the unit cell. Carbon and hydrogen atoms are shown in gray and white, respectively.

Figures S4 and S5 in the Supporting Information). These weak noncovalent intermolecular interactions help lock or rigidify the molecular conformation, preventing the dye molecules from undergoing intramolecular motion and, hence, enabling them to emit strong PL in the crystal state. On the other hand, these forces are easily destroyed by external stimuli, enabling one to change their morphology and, thus, their light emission. Interestingly, the crystal structure of ADHA-c and its ^{1}H NMR spectrum shows the presence of CHCl$_3$ molecules. These molecules may provide a solvent environment for the intramolecular motion of the dye molecules (see Figure S6 in

the Supporting Information). This may be the possible reason why ADHA-c exhibits an abnormal low quantum yield. Indeed, after removal of the solvent molecules by heating at 100 °C under vacuum for 12 h, ADHA-c becomes more emissive, with a higher quantum yield of 26.2% (Figure S7 in the Supporting Information). On the other hand, excluding the effect of molecular size, the smaller occupied space—and, hence, higher packing density in TDHA-g than in TDHA-b—should help to further rigidify the molecular conformation and block the nonradiative pathways, thus resulting in a much higher emission efficiency.

TDHA-am, TDHA-b, and TDHA-g can be interconverted by tuning the molecular packing through the application of the external stimuli; in other words, TDHA shows a multicolor luminescence switching property (see Figure 4, as well as
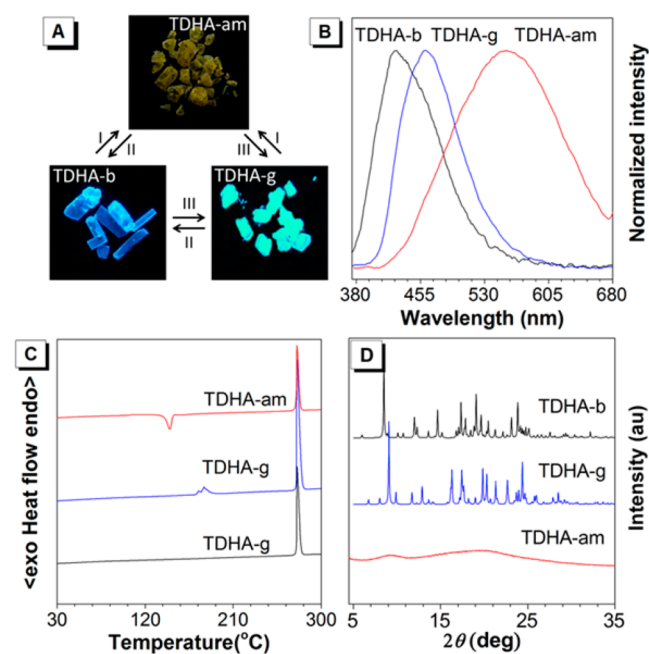
Figure 4. (A) Photographs of TDHA-b, TDHA-g, and TDHA-am and their reversible interconversion under different conditions. (B) PL spectra, (C) DSC thermograms, and (D) powder XRD diffractions of TDHA-b, TDHA-g, and TDHA-am. The photographs were taken under UV illumination. Conditions: heating to melt and cooling by liquid nitrogen (I), heating at 170 °C for more than 1 h or fuming with CH$_2$Cl$_2$ or CHCl$_3$ vapor for 3 h (II), and fuming with acetone vapor for 3 h (III).

Figures S8−S11 in the Supporting Information). By quickly quenching the melts of TDHA-b and TDHA-g, TDHA-am is obtained, as verified by its almost flat powder XRD pattern.

Normally, an amorphous solid will crystallize upon heating or fuming by solvent vapor. This is also true for TDHA-am: its DSC thermogram, which was recorded during the first heating cycle, detected an exothermic peak at 145 °C, which was due to its recrystallization (see Figure S8). Thus, TDHA-am transforms to TDHA-g upon thermal annealing. When it was fumed with CH$_2$Cl$_2$ or CHCl$_3$ vapor, it was converted to TDHA-b. When the solvent was changed to acetone, TDHA-g was finally obtained (Figure S9). Reversible transformation between TDHA-b and TDHA-g can be realized by either heating or vapor fuming. The blue emissive TDHA-b can be obtained by annealing TDHA-g at temperatures below its melting point (180 °C, as determined by differential scanning calorimetry (DSC)). No peak was observed in the DSC curve of TDHA-b before it melts, indicating that it is thermally quite stable (Figure S10). TDHA-b can be obtained also by fuming TDHA-g with CH$_2$Cl$_2$ or CHCl$_3$ vapor. It converts back to TDHA-g by fuming with acetone vapor (Figure S11). Thus, as suggested by the PL spectra shown in Figure 4B, we can switch the emission of TDHA reversibly between three colors (blue, green, and yellow) by fuming or thermal processes. Similarly, the blue emissive ADHA-c and yellow emissive ADHA-am can be reversibly interconverted to each other by repeated grinding/fuming cycles.

Theoretical Calculation. To gain a deeper insight into the polymorphism-dependent emission of the R-DHAs, theoretical calculation was carried out by TD-DFT on B3LYP/6-31G(d) basis set. The aggregation effect was modeled using a quantum mechanics and molecular mechanics (QM/MM) approach. The solid-phase computational models for TDHA-b and TDHA-g were set up based on their crystal structures obtained from X-ray crystallography.[46]

Table 2 shows the dihedral angles in the optimal structures of TDHA-b and TDHA-g at ground and excited states (S_0 and S_1) with carbon atom and angle labels as shown in the TDHA-b structure (Figure 5). The angles in their crystal structures are also provided for comparison. The torsional angles in C2−C1−C12−C13 (θ_4) and C3−C4−C19−C20 (θ_1) involve the rotation of the conjugated phenyl rings, while those in C1−C2−C44−C43, C1−C2−C33−C34 and C4−C3−C39−C40 are associated with the vibration of the 9,10-dihydroanthracene blade. These values change when the molecules are photoexcited. Thus, intramolecular motion should play key roles in the excited-state relaxation. Definitely, efficient restriction of such motion will exert remarkably influence on the light emission process. TDHA-b exhibit larger changes |$\Delta(S_0 − S_1)$| in θ_4 and θ_1 (21.96° and 5.05°) than those in TDHA-g (14.01° and 2.94°). This suggests that its phenyl rings possess greater freedom to undergo rotation in the excited state, thus leading to a lower emission efficiency.

Table 2. Selected Dihedral Angles in the Optimized Geometry and Crystal Structures of TDHA-b and TDHA-g

	TDHA-b				TDHA-g			
	S_0	S_1	|$\Delta(S_1 − S_0)$|	crystal	S_0	S_1	|$\Delta(S_1 − S_0)$|	crystal
C2−C1−C12−C13 (θ_4)	−45.44	−23.48	21.96	−48.51	−43.90	−29.89	14.01	−44.53
C3−C4−C19−C20 (θ_1)	−54.07	−49.02	5.05	−55.64	−45.83	−42.89	2.94	−45.79
C1−C2−C44−C43	−50.00	−41.45	8.55	−49.91	−47.59	−39.12	8.47	−47.11
C1−C2−C33−C34	49.59	45.32	4.27	50.32	42.16	37.36	4.80	42.09
C4−C3−C39−C40	47.07	45.07	2.00	45.44	47.01	44.62	2.39	46.00
C2−C1−C5−C10 (θ_3)	95.50	94.79	0.71	95.97	120.38	122.68	2.30	118.69
C3−C4−C26−C31 (θ_2)	67.78	66.06	1.72	66.65	72.54	70.73	1.81	73.95
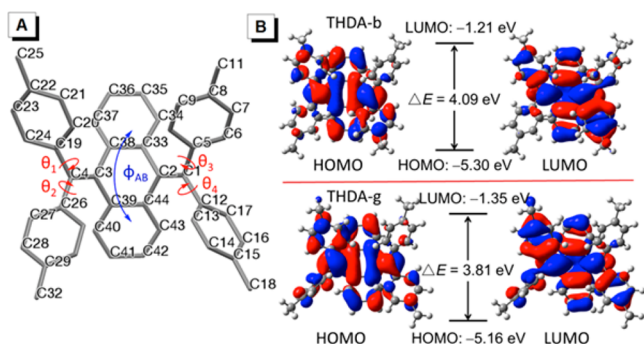
Figure 5. (A) Structure of TDHA-b with labels of carbon atoms and dihedral angles. (B) Spatial plots of HOMO and LUMO of TDHA-b and TDHA-g.

Careful examination of the selected torsional angles in the optimized S_0 and crystal structures reveals that the two sets of data are roughly equal. This indicates the good reliability of the adopted QM/MM approach. However, the absolute values of θ_1, θ_2, θ_3, and θ_4 in TDHA-b and TDHA-g are all larger than 40°, which is suggestive of their contorted structures. The θ_1 and θ_4 values in TDHA-g are smaller than those in TDHA-b. Thus, the former molecule should adopt a more planar structure and process a higher conjugation, which is in agreement with its narrower band gap (3.81 eV), estimated by the equation

$$\Delta E = LUMO - HOMO$$

(see Figure 5). Indeed, from the spatial plots shown in Figure 5, the orbitals from the phenyl groups of TDHA-g contribute slightly more to the electron clouds of HOMO and LUMO than those in TDHA-b. This enables better electronic communication, hence leading to a narrower band gap and red-shifted emission. The calculated vertical excitation energy (VEE), electric transition dipole moment (EDM), and the assignment for S_1 states of TDHA-b and TDHA-g are given in Table S1 in the Supporting Information, together with the available experimental values. In both molecules, the S_1 state is assigned mainly by the transition from HOMO to LUMO. It is noted that the VEE difference for emission between TDHA-b and TDHA-g agree quite well with that of the experimental value, which corresponds to a wavelength shift of ∼40 nm.

CONCLUSION

In summary, we have designed and synthesized a novel class of bis(diarylmethylene)dihydroanthracenes with butterfly shapes. These molecules are AIE-active, because of the restriction of intramolecular motion in the aggregated state. On the other hand, their butterfly-like shapes afford a loose molecular packing with weak noncovalent intermolecular interactions in the crystal state, which enables them to undergo reversible transformation between an efficient bluer-emissive crystal state and weakly redder-emissive amorphous powders by grinding, heating, and solvent fuming processes. Through investigation of their crystal structures and theoretical calculation, the extent of twisting of their molecular structures, packing density, and freedom of intramolecular motion in the excited state are responsible for generating different aggregated states with varied emission color and efficiency. We believe the work presented here not only offers in-depth insights into the mechanochromic process but also can provide a practical way

to analyze and interpret the structure−property relationships in other systems.

ASSOCIATED CONTENT

Ⓢ Supporting Information

. The Supporting Information is available free of charge on the ACS Publications website at DOI: 10.1021/acs.chemmater.5b02280.

Materials and instrumentations; synthesis and characterization of PDHA, ADHA, and TDHA; PL spectra, fluorescent photographs, DSC thermograms and powder X-ray diffraction of the dye molecules; ^{1}H NMR spectra of ADHA crystals; crystals structures of PDHA and ADHA; table showing the theoretical results (PDF)

Crystallographic data for $C_{91}H_{75}Cl_9O_8$ (CIF)

Crystallographic data for $C_{40}H_{28}$ (CIF)

Crystallographic data for monoclinic $C_{44}H_{36}$ (CIF)

Crystallographic data for triclinic $C_{44}H_{36}$ (CIF)

AUTHOR INFORMATION

Corresponding Authors
*E-mail: dongyq@bnu.edu.cn (Y. Q. Dong).
*E-mail: tangbenz@ust.hk (B. Z. Tang).

Author Contributions
†Z.H. and L.Z. contributed equally.

Notes
The authors declare no competing financial interest.

ACKNOWLEDGMENTS

REFERENCES

(1) Chi, Z.; Zhang, X.; Xu, B.; Zhou, X.; Ma, C.; Zhang, Y.; Liu, S.; Xu, J. Recent Advances in Organic Mechano-fluorochromic Materials. *Chem. Soc. Rev.* **2012**, *41*, 3878−3896.

(2) Xu, J.; Chi, Z. *Mechanochromic Fluorescent Materials: Phenomena, Materials and Applications*; Royal Society of Chemistry: London, U.K., 2014.

(3) Sagara, Y.; Kato, T. Mechanically Induced Luminescence Changes in Molecular Assemblies. *Nat. Chem.* **2009**, *1*, 605−610.

(4) Davis, D. A.; Hamilton, A.; Yang, J. L.; Cremar, L. D.; Van Gough, D.; Potisek, S. L.; Ong, M. T.; Braun, P. V.; Martinez, T. J.; White, S. R.; Moore, J. S.; Sottos, N. R. Force-Induced Activation of Covalent Bonds in Mechanoresponsive Polymeric Materials. *Nature* **2009**, *459*, 68−72.

(5) Mao, Z.; Yang, Z.; Mu, Y.; Zhang, Y.; Wang, Y.-F.; Chi, Z.; Lo, C.-C.; Liu, S.; Lien, A.; Xu, J. Linearly Tunable Emission Colors Obtained from a Fluorescent−Phosphorescent Dual-Emission Compound by Mechanical Stimuli. *Angew. Chem., Int. Ed.* **2015**, *54*, 6270−6273.

(6) Xu, S.; Liu, T.; Mu, Y.; Wang, Y.-F.; Chi, Z.; Lo, C.-C.; Liu, S.; Zhang, Y.; Lien, A.; Xu, J. An Organic Molecule with Asymmetric Structure Exhibiting Aggregation-Induced Emission, Delayed Fluo-

rescence, and Mechanoluminescence. *Angew. Chem., Int. Ed.* **2015**, *54*, 874−878.

(7) Li, C.; Tang, X.; Zhang, L.; Li, C.; Liu, Z.; Bo, Z.; Dong, Y. Q.; Tian, Y.-H.; Dong, Y.; Tang, B. Z. Reversible Luminescence Switching of an Organic Solid: Controllable On−Off Persistent Room Temperature Phosphorescence and Stimulated Multiple Fluorescence Conversion. *Adv. Opt. Mater.* **2015**, *3*, 1184.

(8) Li, R.; Xiao, S.; Li, Y.; Lin, Q.; Zhang, R.; Zhao, J.; Yang, C.; Zou, K.; Li, D.; Yi, T. Polymorphism-Dependent and Piezochromic Luminescence Based on Molecular Packing of a Conjugated Molecule. *Chem. Sci.* **2014**, *5*, 3922−3928.

(9) Xu, B.; He, J.; Mu, Y.; Zhu, Q.; Wu, S.; Wang, Y.; Zhang, Y.; Jin, C.; Lo, C.; Chi, Z.; Lien, A.; Liu, S.; Xu, J. Very Bright Mechanoluminescence and Remarkable Mechanochromism Using a Tetraphenylethene Derivative with Aggregation-Induced Emission. *Chem. Sci.* **2015**, *6*, 3236−3241.

(10) Nagura, K.; Saito, S.; Yusa, H.; Yamawaki, H.; Fujihisa, H.; Sato, H.; Shimoikeda, Y.; Yamaguchi, S. Distinct Responses to Mechanical Grinding and Hydrostatic Pressure in Luminescent Chromism of Tetrathiazolylthiophene. *J. Am. Chem. Soc.* **2013**, *135*, 10322−10325.

(11) Gu, X.; Yao, J.; Zhang, G.; Yan, Y.; Zhang, C.; Peng, Q.; Liao, Q.; Wu, Y.; Xu, Z.; Zhao, Y.; Fu, H.; Zhang, D. Polymorphism-Dependent Emission for Di(p-methoxyphenyl)-dibenzofulvene and Analogues: Optical Waveguide/Amplified Spontaneous Emission Behaviors. *Adv. Funct. Mater.* **2012**, *22*, 4862−4872.

(12) Zhang, G.; Lu, J.; Sabat, M.; Fraser, C. L. Polymorphism and Reversible Mechanochromic Luminescence for Solid-State Difluoroboron Avobenzone. *J. Am. Chem. Soc.* **2010**, *132*, 2160−2162.

(13) Wang, K.; Zhang, H.; Chen, S.; Yang, G.; Zhang, J.; Tian, W.; Su, Z.; Wang, Y. Organic Polymorphs: One-Compound-Based Crystals with Molecular-Conformation- and Packing-Dependent Luminescent Properties. *Adv. Mater.* **2014**, *26*, 6168−6173.

(14) Wang, K.; Huang, S.; Zhang, Y.; Zhao, S. S.; Zhang, H. Y.; Wang, Y. Multicolor Fluorescence and Electroluminescence of an ICT-type Organic Solid Tuned by Dodulating the Accepting Nature of the Central Core. *Chem. Sci.* **2013**, *4*, 3288−3293.

(15) Wang, L.; Wang, K.; Zou, B.; Ye, K.; Zhang, H.; Wang, Y. Luminescent Chromism of Boron Diketonate Crystals: Distinct Responses to Different Stresses. *Adv. Mater.* **2015**, *27*, 2918−2922.

(16) Dong, Y.; Xu, B.; Zhang, J.; Tan, X.; Wang, L.; Chen, J.; Lv, H.; Wen, S.; Li, B.; Ye, L.; Zou, B.; Tian, W. Piezochromic Luminescence Based on the Molecular Aggregation of 9,10-Bis((E)-2-(pyrid-2-yl)vinyl)anthracene. *Angew. Chem., Int. Ed.* **2012**, *51*, 10782−10785.

(17) Luo, X.; Li, J.; Li, C.; Heng, L.; Dong, Y. Q.; Liu, Z.; Bo, Z.; Tang, B. Z. Reversible Switching of the Emission of Diphenyldibenzofulvenes by Thermal and Mechanical Stimuli. *Adv. Mater.* **2011**, *23*, 3261−3265.

(18) Zhang, H. Y.; Zhang, Z. L.; Ye, K. Q.; Zhang, J. Y.; Wang, Y. Organic Crystals with Tunable Emission Colors Based on a Single Organic Molecule and Different Molecular Packing Structures. *Adv. Mater.* **2006**, *18*, 2369−2372.

(19) Gu, X.; Yao, J.; Zhang, G.; Zhang, D. Controllable Self-Assembly of Di(p-methoxyphenyl)Dibenzofulvene into Three Different Emission Forms. *Small* **2012**, *8*, 3406−3411.

(20) Hu, F.; Zhang, G.; Zhan, C.; Zhang, W.; Yan, Y.; Zhao, Y.; Fu, H.; Zhang, D. Highly Solid-State Emissive Pyridinium-Substituted Tetraphenylethylene Salts: Emission Color-Tuning with Counter Anions and Application for Optical Waveguides. *Small* **2015**, *11*, 1335−1344.

(21) Shi, H.; Liu, Z.; Geng, J.; Tang, B. Z.; Liu, B. Specific Detection of Integrin $\alpha_v\beta_3$ by Light-Up Bioprobe with Aggregation-Induced Emission Characteristics. *J. Am. Chem. Soc.* **2012**, *134*, 9569−9572.

(22) Yuan, Y.; Kwok, R. T. K.; Tang, B. Z.; Liu, B. Targeted Theranostic Platinum(IV) Prodrug with a Built-In Aggregation-Induced Emission Light-Up Apoptosis Sensor for Noninvasive Early Evaluation of Its Therapeutic Responses *In Situ*. *J. Am. Chem. Soc.* **2014**, *136*, 2546−2554.

(23) Wang, J.; Mei, J.; Hu, R.; Sun, J. Z.; Qin, A.; Tang, B. Z. Click Synthesis, Aggregation-Induced Emission, E/Z Isomerization, Self-Organization, and Multiple Chromisms of Pure Stereoisomers of a Tetraphenylethene-Cored Luminogen. *J. Am. Chem. Soc.* **2012**, *134*, 9956−9966.

(24) Yang, Z.; Qin, W.; Lam, J. W. Y.; Chen, S.; Sung, H. H. Y.; Williams, I. D.; Tang, B. Z. Fluorescent pH Sensor Constructed from a Heteroatom-Containing Luminogen with Tunable AIE and ICT Characteristics. *Chem. Sci.* **2013**, *4*, 3725−3730.

(25) Hong, Y.; Lam, J. W. Y.; Tang, B. Z. Aggregation-Induced Emission. *Chem. Soc. Rev.* **2011**, *40*, 5361−5388.

(26) Hong, Y.; Lam, J. W. Y.; Tang, B. Z. Aggregation-Induced Emission: Phenomenon, Mechanism and Applications. *Chem. Commun.* **2009**, 4332−4353.

(27) Hu, R.; Leung, N. L. C.; Tang, B. Z. AIE Macromolecules: Syntheses, Structures and Functionalities. *Chem. Soc. Rev.* **2014**, *43*, 4494−4562.

(28) Mei, J.; Hong, Y.; Lam, J. W. Y.; Qin, A.; Tang, Y.; Tang, B. Z. Aggregation-Induced Emission: The Whole Is More Brilliant than the Parts. *Adv. Mater.* **2014**, *26*, 5429−5479.

(29) Leung, N. L. C.; Xie, N.; Yuan, W.; Liu, Y.; Wu, Q.; Peng, Q.; Miao, Q.; Lam, J. W. Y.; Tang, B. Z. Restriction of Intramolecular Motions: The General Mechanism behind Aggregation-Induced Emission. *Chem.—Eur. J.* **2014**, *20*, 15349−15353.

(30) Nishiuchi, T.; Tanaka, K.; Kuwatani, Y.; Sung, J.; Nishinaga, T.; Kim, D.; Iyoda, M. Solvent-Induced Crystalline-State Emission and Multichromism of a Bent π-Surface System Composed of Dibenzocyclooctatetraene Units. *Chem.—Eur. J.* **2013**, *19*, 4110−4116.

(31) Yuan, W. Z.; Tan, Y.; Gong, Y.; Lu, P.; Lam, J. W. Y.; Shen, X. Y.; Feng, C.; Sung, H. H.-Y.; Lu, Y.; Williams, L. D.; Sun, J. Z.; Zhang, Y.; Tang, B. Z. Synergy between Twisted Conformation and Effective Intermolecular Interactions: Strategy for Efficient Mechanochromic Luminogens with High Contrast. *Adv. Mater.* **2013**, *25*, 2837−2843.

(32) Xu, B.; Chi, Z.; Li, H.; Zhang, X.; Li, X.; Liu, S.; Zhang, Y.; Xu, J. Synthesis and Properties of Aggregation-Induced Emission Compounds Containing Triphenylethene and Tetraphenylethene Moieties. *J. Phys. Chem. C* **2011**, *115*, 17574−17581.

(33) He, J. T.; Xu, B.; Chen, F. P.; Xia, H. J.; Li, K. P.; Ye, L.; Tian, W. Aggregation-Induced Emission in the Crystals of 9,10-Distyrylanthracene Derivatives: The Essential Role of Restricted Intramolecular Torsion. *J. Phys. Chem. C* **2009**, *113*, 9892−9899.

(34) Dou, C.; Han, L.; Zhao, S.; Zhang, H.; Wang, Y. Multi-Stimuli-Responsive Fluorescence Switching of a Donor−Acceptor π-Conjugated Compound. *J. Phys. Chem. Lett.* **2011**, *2*, 666−670.

(35) Xu, B.; Chi, Z.; Zhang, X.; Li, H.; Chen, C.; Liu, S.; Zhang, Y.; Xu, J. A New Ligand and Its Complex with Multi-stimuli-Responsive and Aggregation-Induced Emission Effects. *Chem. Commun.* **2011**, *47*, 11080−11082.

(36) Banal, J. L.; White, J. M.; Ghiggino, K. P.; Wong, W. W. H. Concentrating Aggregation-Induced Fluorescence in Planar Waveguides: A Proof-of-Principle. *Sci. Rep.* **2014**, *4*, 4635.

(37) He, Z.; Shan, L.; Mei, J.; Wang, H.; Lam, J. W. Y.; Sung, H. H. Y.; Williams, I. D.; Gu, X.; Miao, Q.; Tang, B. Z. Aggregation-Induced Emission and Aggregation-Promoted Photochromism of Bis-(diphenylmethylene)dihydroacenes. *Chem. Sci.* **2015**, *6*, 3538−3543.

(38) Pola, S.; Kuo, C.-H.; Peng, W.-T.; Islam, M. M.; Chao, I.; Tao, Y.-T. Contorted Tetrabenzocoronene Derivatives for Single Crystal Field Effect Transistors: Correlation between Packing and Mobility. *Chem. Mater.* **2012**, *24*, 2566−2571.

(39) Yu, G.; Yin, S.; Liu, Y.; Chen, J.; Xu, X.; Sun, X.; Ma, D.; Zhan, X.; Peng, Q.; Shuai, Z.; Tang, B.; Zhu, D.; Fang, W.; Luo, Y. Structures, Electronic States, Photoluminescence, and Carrier Transport Properties of 1,1-Disubstituted 2,3,4,5-Tetraphenylsiloles. *J. Am. Chem. Soc.* **2005**, *127*, 6335−6346.

(40) Peng, Q.; Yi, Y.; Shuai, Z.; Shao, J. Toward Quantitative Prediction of Molecular Fluorescence Quantum Efficiency: Role of Duschinsky Rotation. *J. Am. Chem. Soc.* **2007**, *129*, 9333−9339.

(41) Deng, C.; Niu, Y.; Peng, Q.; Qin, A.; Shuai, Z.; Tang, B. Z. Theoretical Study of Radiative and Non-Radiative Decay Processes in Pyrazine Derivatives. *J. Chem. Phys.* **2011**, *135*, 014304.

(42) CCDC 1024629, CCDC 1062138, CCDC 1062139 and CCDC 1062140 contain the supplementary crystallographic data for PDHA, TDHA-b, TDHA-g and ADHA, respectively. These data can be obtained free of charge from the Cambridge Crystallographic Data Centre via ww.ccdc.cam.ac.uk/data_request/cif.

(43) Luo, X.; Zhao, W.; Shi, J.; Li, C.; Liu, Z.; Bo, Z.; Dong, Y. Q.; Tang, B. Z. Reversible Switching Emissions of Tetraphenylethene Derivatives among Multiple Colors with Solvent Vapor, Mechanical, and Thermal Stimuli. *J. Phys. Chem. C* **2012**, *116*, 21967−21972.

(44) Cheng, X.; Li, F.; Han, S.; Zhang, Y.; Jiao, C.; Wei, J.; Ye, K.; Wang, Y.; Zhang, H. Emission Behaviors of Unsymmetrical 1,3-Diaryl-b-diketones: A Model Perfectly Disclosing the Effect of Molecular Conformation on Luminescence of Organic Solids. *Sci. Rep.* **2015**, *5*, 9140.

(45) Cheng, X.; Wang, K.; Huang, S.; Zhang, H.; Zhang, H.; Wang, Y. Organic Crystals with Near-Infrared Amplified Spontaneous Emissions Based on 2′-Hydroxychalcone Derivatives: Subtle Structure Modification but Great Property Change. *Angew. Chem., Int. Ed.* **2015**, *54*, 8369−8373.

(46) Zhang, T.; Jiang, Y.; Niu, Y.; Wang, D.; Peng, Q.; Shuai, Z. Aggregation Effects on the Optical Emission of 1,1,2,3,4,5-Hexaphenylsilole (HPS): A QM/MM Study. *J. Phys. Chem. A* **2014**, *118*, 9094−9104.